Calculation of partition functions and macroscopic properties for a gas-phase reaction from ab initio electronic structure data

Nicolás Rojo Esteban

1 Introduction

Hydrocarbons play a fundamental role in modern society, particularly in the energy and chemical industries, as they form the basis of most fossil fuels and many petrochemical raw materials[1]. A crucial aspect of their chemical behavior is their reaction with oxygen, which underlies combustion for energy generation as well as various atmospheric phenomena, such as pollutant formation and the oxidation of organic compounds in the atmosphere. In this context, methane (CH_4) stands out as the simplest hydrocarbon and a key fuel, being the main component of natural gas. Its reaction with an oxygen atom is an important case study for understanding the initial oxidation mechanisms of hydrocarbons[2].

$$CH_4(g) + O(g) \rightarrow CH_3(g) + OH(g) \quad (1)$$

Therefore, the objective of this work is to analyze the CH_4 + O reaction from a computational perspective, aiming to elucidate its reaction mechanism and evaluate its fundamental thermodynamic properties.

2 Methodology

The methodology employed is based on ab initio computational chemistry calculations. First, the geometries of all species involved in the reaction—including the reactants (methane and the oxygen atom), possible products, and the corresponding transition state—are optimized. This is done using the UMP2 method (Unrestricted Møller-Plesset second-order perturbation theory)[3] combined with a 6-311G(d,p) basis set. This theoretical level is chosen to accurately describe the electronic structure of an open-shell (radical) system like the present one, ensuring reliable geometries for both energy minima (reactants and products) and the saddle point or transition state.

Next, to obtain the thermodynamic properties of the reaction, the Hessian matrix (second derivatives of the energy) is computed for each optimized structure. This calculation provides the vibrational frequencies of each species, which serve two fundamental purposes: to confirm the nature of each stationary point—particularly verifying that the transition state presents a single imaginary frequency, indicative of a maximum energy point on the potential energy surface—and to obtain the necessary thermal corrections (zero-point energy, enthalpic, and entropic corrections) to evaluate thermodynamic functions.

Using the vibrational information and the calculated electronic energies, key reaction parameters can be determined. Specifically, the activation energy (energy difference between reactants and the transition state) is estimated, and the variations in enthalpy and entropy associated with the chemical process are computed. Finally, the Gibbs free energy of the reaction is obtained. These data allow for a detailed characterization of the energy profile of methane's reaction with an oxygen atom, assessing its feasibility and spontaneity under different conditions.

3 Computational details

All geometry optimizations and thermodynamic property calculations were performed using GAMESS[4], employing the UMP2 method with the 6-311G(d,p) basis set. The convergence tolerance for the calculations was set to 10^{-5} Hartree/Bohr, with a maximum of 500 steps for the geometry optimization. For each SCF cycle, a maximum of 99 iterations was allowed to ensure electronic convergence. Additionally, the KiSThelP [5] program was used to compute some thermodynamic properties, including Gibbs free energy, entropy, and equilibrium constants.

4 Results

4.1 Geometry optimization of reactants, transition state and products

Table 1: Comparison of expected and obtained spin values for each species.

Species	Expected Spin (S)	Expected S^2	Obtained S^2	Consistency
CH_4 ($^1A_1$)	0	0.000	0.000	✓
CH_3 ($^2A_2$")	1/2	0.750	0.762	∼
OH ($^2\Pi$)	1/2	0.750	0.755	∼
O (^3P)	1	2.000	2.005	✓
TS	1	2.000	2.048	∼

The Table 1 contains the obtained values of the spin state for the different molecules. For CH_4, the obtained values match perfectly with the expected ones, confirming that it is a singlet state ($S = 0$). In the case of CH_3 and OH, there is a minor deviation in the calculated S^2.

The oxygen atom (O ^3P) shows an expected triplet state with an almost perfect S^2 value of 2.005. The transition state (TS) exhibits a slightly larger deviation (2.048 instead of 2.000), but it remains within an acceptable range.

Table 2: Optimized geometry parameters for CH_4.

C-H Distance (Å)	H-C-H Bond Angle (°)
1.0898	109.47

The optimized geometry of the CH_4 molecule was compared to the experimental data, showing a very close agreement. The experimental C-H bond distance is reported as 1.087 Å[6], while the obtained value from the calculations is 1.0898 Å. The H-C-H bond angle remains consistent with the experimental reference which is exactly 109.47°[6].

It is important to note that the C-H bond distance provided in Table 2 is an average of the four individual C-H bonds. These bond lengths are nearly identical; however, minor discrepancies arise beyond the fourth decimal place. This deviation is attributed to the symmetry group used in the computational calculations. While the CH_4 molecule ideally belongs to the T_d symmetry group, the calculations were performed within the C_1 symmetry framework. The lack of strict tetrahedral

symmetry in the computational model introduces small numerical differences in bond lengths.

Despite this minor variation, the optimized geometry closely matches the expected tetrahedral structure, confirming the reliability of the applied computational method.

Table 3: Optimized geometry parameters for CH_3.

C-H Distance (Å)	**H-C-H Bond Angle (°)**
1.0788	120

The optimized geometry of the CH_3 radical was compared with experimental data, showing excellent agreement. The experimental C-H bond length is reported as 1.072 Å[6], while the calculated value is 1.0788 Å. The H-C-H bond angle remains at 120.0°, consistent with the expected trigonal planar structure.

Unlike the case of CH_4, in this optimization, all three C-H bond distances were found to be exactly equal, and the molecule exhibited a perfect equilateral triangular geometry. This confirms that the calculations accurately preserved the expected D_{3h} symmetry of the CH_3 radical.

The small difference in bond length compared to the experimental value is likely due to basis set limitations or in the computational method. However, the overall structural agreement validates the reliability of the computational approach used.

Table 4: Calculated bond distance of the OH radical.

O-H Distance (Å)	**O-H Bond Angle (°)**
0.9675	-

The calculated bond distance for the OH radical is 0.9675 Å, while the experimental value is 0.970 Å.The $C_{\infty v}$ symmetry of the OH radical ensures that only a single bond length is relevant, making this comparison straightforward. The negligible deviation suggests that the computational method employed provides a reliable approximation of the experimental geometry.

Table 5: Optimized geometry parameters for CH_3OH.

Parameter	**Value**
O-H Distance	1.1821 Å
C-H Distance	1.2855 Å
C-H' Distance	1.0867 Å
C-H" Distance	1.0867 Å
C-H"' Distance	1.062 Å
H'-C-H Angle	104.16°
C-H-O Angle	177.88°

The optimized geometry of CH_3OH was analyzed and compared with the expected experimental values. The O-H bond length obtained from the calculations is 1.1821 Å, slightly shorter than the experimental value of 1.206 Å[7]. Similarly, the C-H bond length is calculated as 1.2855 Å, which also shows a minor deviation from the reference value of 1.254 Å[7]. The three remaining C-H bonds exhibit slight variations, but remain close to the experimental values of 1.080Å[7].

The calculated angles show that the H'-C-H bond angle is 104.16°, which is in good agreement with the reference value of 104.7°[6]. The C-H-O bond angle is computed as 177.88°, which is very close to the expected 180.0°, confirming that the molecule retains a nearly linear alignment in this region.

4.2 Thermodinamic and vibrational calculations

Table 6: Electronic energies and zero-point energies (ZPE) at UMP2/6-311G(d,p) level.

Species	**Energy** (kcal/mol)	**ZPE** (kcal/mol)
CH_3	-24917.22329859	28.545
CH_4	-25338.90282503	0
OH	-47424.85246679	18.905
O	-47014.14766925	5.499
TS	-72331.34800026	24.701

Using the electronic and zero-point energies (ZPE) reported in Table 6, we calculated the energy differences between reactants and products as well as the activation energy. The calculations were performed both with and without considering the ZPE corrections.

The electronic energy difference between reactants and products is calculated as:

$$\Delta_r\varepsilon = \sum_i^{products} \varepsilon_i - \sum_j^{reactants} \varepsilon_j \tag{2}$$

The activation energy, without considering ZPE, is given by:

$$\Delta\varepsilon^{\neq} = \varepsilon_{TS} - \sum_j^{reactants} \varepsilon_j \tag{3}$$

And then, we took into account the effect of the zero-point energy (ZPE):

$$\Delta_r\varepsilon(ZPE) = \sum_i^{products} (\varepsilon_i + ZPE_i) - \sum_j^{reactants} (\varepsilon_j + ZPE_j) \tag{4}$$

$$\Delta\varepsilon^{\neq}(ZPE) = \varepsilon_{TS} + ZPE_{TS} - \sum_j^{reactants} (\varepsilon_j + ZPE_j) \tag{5}$$

Table 7 presents the computed energy differences:

Table 7: Energy differences for the reaction, computed with and without ZPE correction.

Energy Difference	**Value (kcal/mol)**
$\Delta\varepsilon$ (no ZPE)	10.978
$\Delta\varepsilon^{\neq}$ (no ZPE)	21.702
$\Delta\varepsilon$ (with ZPE)	6.834
$\Delta\varepsilon^{\neq}$ (with ZPE)	17.858

Table 8: standard gibbs free energy corrections and total standard gibbs free energy for CH_4 at different temperatures.

T (K)	G°_{corr} (kcal/mol)	$G^{\circ}_{CH_4}$ (kcal/mol)
0.001	28.545	-25310.358
300	16.116	-25322.787
600	0.194	-25338.709
900	-17.575	-25356.478

Experimental values for the activation energy ($\Delta\varepsilon^{\neq}$) and reaction energy difference ($\Delta\varepsilon$) provide a useful comparison. Arrhenius rate constant experiments within the temperature range of 400-575 K yield a value of $\Delta\varepsilon^{\neq}$(ZPE) = (9.3 ± 1.2) kcal/mol[8]. Additionally, higher-level calculations using PUMP4//UMP2/6-311G(3d2f,3p2d) predict $\Delta\varepsilon^{\neq}$(ZPE) = 9.4 kcal/mol[7], aligning well with experimental findings.

Comparing our results, we observe that our computed activation energy with ZPE (17.858 kcal/mol) overestimates the experimental and higher-level computational values (9.4 kcal/mol)[7]. This discrepancy suggests that using a more extensive basis set and a higher-order perturbative method would improve accuracy. Similarly, our computed reaction energy difference ($\Delta\varepsilon$) with ZPE (6.834 kcal/mol) is significantly higher than the experimental value of 1.3 kcal/mol[7], reinforcing the need for methodological improvements.

Overall, the computed values are overestimated compared to experimental data, highlighting the limitations of the current computational method.

To determine additional thermodynamic properties, it is necessary to compute the eigenvalues of the Hessian matrix. These eigenvalues account for translational, rotational, and vibrational motion. In the case of atoms, which lack bonds capable of vibrating or rotating, the Hessian matrix exclusively describes translational motion along with electronic contributions. Furthermore, the Hessian matrix plays a crucial role in refining thermodynamic properties, including enthalpy (H) and standard gibbs free energy (G), and can also be used to derive entropy (S) directly.

We begin by examining the standard gibbs free energy (G) and entropy (S) of the species under standard conditions of 1 bar pressure across different temperatures. The standard gibbs free energy of each species is obtained by incorporating a correction energy to the computed electronic energy of the molecules. Since the Gibbs energy correction, denoted as G_{corr}, inherently accounts for the Zero Point Energy (ZPE) of the system, it is essential to employ the UMP2 electronic energy in calculations. It should be emphasized that the standard standard gibbs free energy (G^0) varies with temperature but remains independent of pressure.

- CH_4: The computed standard gibbs free energy values for methane are presented in Table 8.

Methane (CH_4) is a non-linear molecule, meaning that it is expected to exhibit $3N-6$ normal modes of vibration, where N represents the number of atoms. Based on this formula, methane should have nine vibrational modes. However, upon diagonalization of the Hessian matrix, 15 frequency modes are obtained (see Table 9), leading to an apparent discrepancy.

This difference is explained by the total degrees of freedom within a molecule. In general, a molecule has $3N$ degrees of freedom: three are associated with translational motion (movement along the x, y, and z axes), three correspond to rotational motion (rotation about these axes, provided the molecule is non-linear), and the remaining $3N-6$ degrees of freedom correspond to vibrational motion.

Thus, the Hessian matrix diagonalization provides all $3N$ degrees of freedom, encompassing translational, rotational, and vibrational contributions. According to the literature, vibrational modes for methane appear above 1300 cm^{-1} [**?**]. Therefore, the six lower-frequency modes observed in the calculations are assigned to translational and rotational motions, rather than vibrational ones.

Table 9: Vibrational frequencies, symmetry, and IR intensities for CH_4 at UMP2/6-311G(d,p).

Frequency (cm^{-1})	**Symmetry**	**IR Intensity**
23.69	A	0.00000
22.48	A	0.00000
20.05	A	0.00000
0.47	A	0.00000
0.52	A	0.00000
1.37	A	0.00000
1365.02	A	0.32991
1365.07	A	0.32993
1365.08	A	0.32988
1582.68	A	0.00000
1582.71	A	0.00000
3074.09	A	0.00000
3210.87	A	0.52098
3210.93	A	0.52098
3211.00	A	0.52099

- O: The calculated Gibbs free energies for the oxygen atom are presented in 10

Table 10: Standard Gibbs free energies of the O atom calculated at UMP2/6-311G(d,p) level at different temperatures.

T (K)	G°_{corr} (kcal/mol)	G°_{O} (kcal/mol)
0.001	0.000	-47014.148
300	-9.450	-47023.598
600	-20.966	-47035.114
900	-33.262	-47047.410

Since oxygen is only an atom it does not have normal modes of vibration.

- CH_3:

  The calculated Gibbs free energies for the CH_3 radical are presented in 11

Table 11: Standard Gibbs free energies of the CH_3 radical calculated at UMP2/6-311G(d,p) level at different temperatures.

T (K)	G°_{corr} (kcal/mol)	$G^{\circ}_{CH_3}$ (kcal/mol)
0.001	18.905	-24898.318
300	6.364	-24910.859
600	-9.926	-24927.149
900	-27.992	-24945.215

Table 12: Vibrational frequencies, symmetry, and IR intensities for CH_3 at UMP2/6-311G(d,p).

Frequency (cm^{-1})	**Symmetry**	**IR Intensity**
14.19	A	0.00000
0.07	A	0.00000
0.00	A	0.00000
6.50	A	0.00000
15.89	A	0.00000
15.92	A	0.00000
421.09	A	1.95292
1452.14	A	0.06973
1452.33	A	0.06966
3171.35	A	0.00000
3363.66	A	0.10525
3363.75	A	0.10524

The diagonalization of the Hessian yields 12 frequencies (see Table 12), but as noted in the literature [**?**], only the six above 400 cm^{-1} correspond to vibrational modes. The remaining six are associated with translational and rotational motions.

Furthermore, the presence of nearly degenerate modes suggests a high degree of molecular symmetry, reinforcing the structural characteristics expected for this species.

- OH: The calculated Gibbs free energies for the OH radical are presented in table 13

Table 13: standard gibbs free energy corrections and total standard gibbs free energy for OH at different temperatures.

T (K)	G°_{corr} (kcal/mol)	G°_{OH} (kcal/mol)
0.001	5.499	-47419.353
300	-5.192	-47430.044
600	-18.776	-47443.628
900	-33.455	-47458.307

Table 14: Vibrational frequencies, symmetry, and IR intensities for OH at UMP2/6-311G(d,p).

Frequency (cm^{-1})	**Symmetry**	**IR Intensity**
21.20	A	3.53716
0.00	A	0.00000
0.00	A	0.00000
0.00	A	0.00000
42.95	A	3.53538
3846.55	A	0.23603

The OH is a linear molecule, so it has only one normal mode of vibration, corresponding to the stretching of the OH bond. According to the literature, this mode appears above 3800 cm^{-1} [6]. The remaining six frequencies correspond to rotational and translational motions.

- CH_3OH(TS): The calculated Gibbs free energies for the transition state (TS) are presented in table 15

Table 15: Standard Gibbs free energies of the TS molecule calculated at UMP2/6-311G(d,p) level at different temperatures.

T (K)	G°_{corr} (kcal/mol)	G°_{TS} (kcal/mol)
0.001	24.701	-72306.647
300	9.022	-72322.326
600	-11.391	-72342.739
900	-34.606	-72365.954

Table 16: Vibrational frequencies, symmetry, and IR intensities for TS at UMP2/6-311G(d,p).

Frequency (cm^{-1})	**Symmetry**	**IR Intensity**
2205.48 I	A	49.60144
106.87	A	0.00328
11.87	A	0.05338
10.65	A	0.05932
0.14	A	0.00000
7.10	A	0.01996
12.35	A	0.00557
301.82	A	0.08657
370.28	A	0.03580
610.89	A	0.21811
1063.41	A	0.58867
1141.52	A	0.81133
1243.64	A	0.29657
1427.36	A	0.01407
1463.47	A	0.09622
3117.82	A	0.04470
3264.81	A	0.13319
3273.62	A	0.11747

The vibrational analysis of the transition state (TS) at the UMP2/6-311G(d,p) level reveals a total of 18 vibrational frequencies (see Table 16). Among these, one imaginary frequency at 2205.48 cm^{-1} confirms the nature of the transition state. This imaginary frequency indicates the presence of a saddle point on the potential energy surface

The remaining frequencies are all positive, confirming that the structure is indeed a first-order transition state. The lower-frequency modes (below 300 cm^{-1}), which are 6 modes ,correspond to translational and rotational contributions, while the higher-frequency modes, which are 12, represent genuine vibrational motions of the molecular structure.

Unlike standard gibbs free energy, entropy is directly obtained from the GAMESS output without requiring any corrections. Since entropy is not an energy quantity, it does not necessitate adjustments like standard gibbs free energy does. The entropy values for all species analyzed in this study are presented in Table 17.

Table 17: Standard entropy values S° studied at different temperatures in cal/(mol·K).

T (K)	CH_4	O	CH_3	OH	TS
0.001	-50.879	-26.186	-50.782	-45.123	-41.075
300	49.449	36.468	50.391	42.592	62.309
600	56.346	39.912	57.607	47.415	73.152
900	61.971	41.926	62.616	50.264	81.292

The results in Table 17 demonstrate that entropy values increase with temperature for all species. This trend aligns with thermodynamic principles, as higher temperatures lead to greater molecular disorder and an increased number of accessible microstates. Among the analyzed species, the transition state (TS) consistently exhibits the highest entropy at all temperatures, which is expected due to its less constrained structure compared to stable reactants and products. Conversely, atomic oxygen (O) has the lowest entropy, as expected for a monoatomic species with minimal degrees of freedom. The differences in entropy values between CH_4, CH_3, and OH reflect their distinct molecular structures and vibrational contributions, with CH_4 displaying the highest entropy among them due to its greater number of vibrational modes.

Table 18: Canonical partition function values Q (no dimension) studied at different temperatures.

T (K)	Q_{CH_4}	Q_{CH_3}	Q_{OH}	Q_O	Q_{TS}
0.001	$1.39 \cdot 10^{-13}$	$1.46 \cdot 10^{-13}$	$4.15 \cdot 10^{-12}$	$1.55 \cdot 10^{7}$	$1.93 \cdot 10^{-11}$
300	$1.13 \cdot 10^{9}$	$1.37 \cdot 10^{9}$	$6.14 \cdot 10^{7}$	$7.66 \cdot 10^{6}$	$2.64 \cdot 10^{11}$
600	$2.12 \cdot 10^{10}$	$3.17 \cdot 10^{10}$	$6.95 \cdot 10^{8}$	$4.33 \cdot 10^{7}$	$1.40 \cdot 10^{13}$
900	$1.58 \cdot 10^{11}$	$2.44 \cdot 10^{11}$	$2.88 \cdot 10^{9}$	$1.19 \cdot 10^{8}$	$2.52 \cdot 10^{14}$

All thermodynamic calculations in this study have been performed using the canonical ensemble, where the number of particles (N), temperature (T), and volume (V) remain constant. This choice ensures a well-defined statistical framework for computing thermodynamic properties, as it accurately describes isolated molecular systems at thermal equilibrium.

One of the key quantities obtained from these calculations is the partition function, which plays a fundamental role in statistical thermodynamics. The partition function gives information about the accessible energy levels of a system and allows for the computation of other thermodynamic properties such as entropy, enthalpy, and standard gibbs free energy. GAMESS provides the values of the partition function at different temperatures,showed in Table 18.

4.3 Calculation of thermodynamic properties: $\Delta G^{\neq}, \Delta G^0, \Delta_r S^0, K_{eq}$

To obtain the variation in the standard gibbs free energy we can use equation 6

$$\Delta G^{0\neq} = G^0_{TS} - \sum_{i}^{\text{reactants}} G^0_i \tag{6}$$

Table 19: Calculated values for the standard gibbs free energy change of activation for the reaction. There's no experimental data about this parameter.

T (K)	$\Delta_r G^{\neq}_{calc}$ (kcal/mol)	$\Delta_r G^{\neq}_{exp}$ (kcal/mol)
0.001	17.858	-
300	24.058	-
600	31.083	-
900	37.933	-

The calculated values for the standard gibbs free energy of activation are in Table 19. As it is shown the standard gibbs free energy increases with the rise in temperature. There are no experimental data available to compare.

To calculate the standard gibbs free energy of the reaction we can use the equation 7

$$\Delta_r G^0 = \sum_j^{\text{products}} G_j^0 - \sum_i^{\text{reactants}} G_i^0 \tag{7}$$

Table 20: Calculated and experimental variations of the standard gibbs free energy of the reaction at various temperatures.[6]

T (K)	$\Delta_r G^\circ_{calc}$ (kcal/mol)	$\Delta_r G^\circ_{exp}$ (kcal/mol)
0.001	6.834	1.8
300	5.481	0.3
600	3.045	-2.2
900	0.365	-4.8

The values for the calculated and experimental standard gibbs free energy [6] of the reaction are presented in Table 20. As observed, the calculated values do match the experimental ones. The discrepancy in the calculations can be attributed to several factors.

One possible source of error is the overestimation of the electronic energy in the calculations, as previously highlighted in Table 7. Since the standard gibbs free energy is derived from the electronic energy.

Another potential cause of this discrepancy is the precision of the Gibbs energy correction applied in the calculations. This correction depends on the value of the canonical partition function. The correction terms used may not fully capture all thermodynamic contributions, leading to deviations from experimental results.

The difference in entropy of the reaction can be calculated using equation 8

$$\Delta_r S^\circ = \sum_j^{\text{products}} S_j^\circ - \sum_i^{\text{reactants}} S_i^\circ \tag{8}$$

Table 21: Experimental and calculated values for the entropy difference of the reaction at different temperatures.[6]

T (K)	$\Delta_r S^\circ_{calc}$ (cal/mol K)	$\Delta_r S^\circ_{exp}$ (cal/mol K)
0.001	-18.840	-
300	7.066	7.3
600	8.764	8.8
900	8.983	8.9

The table 21 presents the calculated and experimental values for the entropy variation[6]. The strong agreement between these values suggests that the computational approach provides an accurate estimation of entropy changes.

Entropy is determined using the canonical partition function, reinforcing the idea that discrepancies in the standard gibbs free energy variation are unlikely to come from thermodynamic corrections. Instead, these deviations are more plausibly linked to the electronic energy values used in the calculations. Since standard gibbs free energy is a sum of both electronic and thermal contributions, inaccuracies in the electronic energy can significantly affect the final results.

Finally to calculate the values of the K_{eq} we can use equation 9

$$K_{eq} = e^{-\frac{\Delta_r G^\circ}{RT}} \tag{9}$$

Table 22: Experimental and calculated values for the K_{eq} at different temperatures. [6]

T (K)	K_{eq} (calculated)	K_{eq}(exp.)
0.001	0	0.0
300	0.991	0.6
600	0.997	6.2
900	1.000	15.0

The table 22 contains the values of the calculated K_eq. As we can see the results are very different from the experimental values since as we can see in equation 9, this calculated values depend exponentially on the standard gibbs free energy which is not very precise.

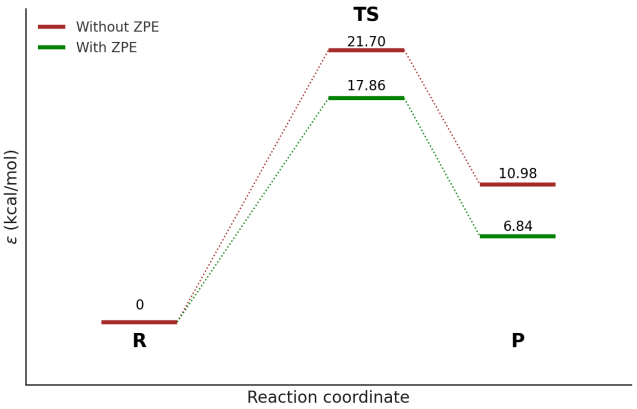

Figure 1: Electronic energy profile of the reaction

In figure 1 the electronic energy profile of the reaction is plotted and we can see that the products have more energy than the reactants.

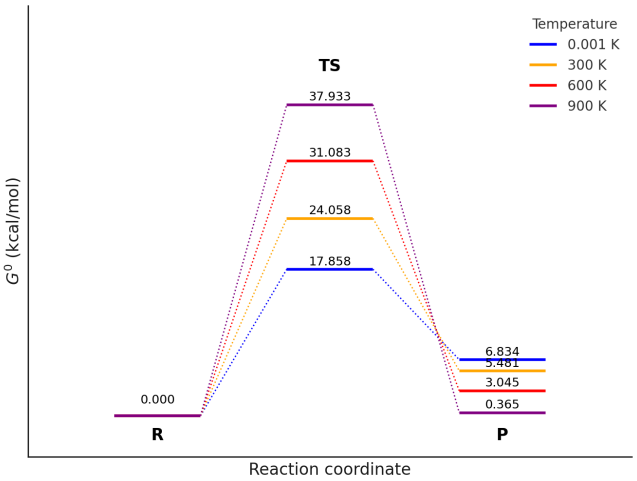

Figure 2: standard gibbs free energy profile of the reaction

As we can see in figure 2 the standard gibbs free energy of the transition state increases with the temperature whereas the standard gibbs free energy of the products decreases with the temperature.

4.4 Calculations of the thermodinamic properties using KiSThelP

Table 23: Gibbs Free Energy ($\Delta_r G^\circ$) calculated with KiSThelP and experimental values

T (K)	ΔG_{calc} (kcal/mol)	ΔG_{exp} (kcal/mol)
0.001	28.59	1.8
300	22.93	0.3
600	12.74	-2.2
900	1.52	-4.8

Table 24: Entropy ($\Delta_r S^\circ$) calculated with KiSThelP and experimental values

T (K)	ΔS_{calc} (cal/mol·K)	ΔS_{exp} (cal/mol·K)
0.001	-78.82	-
300	29.58	7.3
600	36.68	8.8
900	37.59	8.9

Table 25: Equilibrium Constant (K_{eq}) calculated with KiSThelP and experimental values

T (K)	$K_{eq,calc}$	$K_{eq,exp}$
0.001	0.00×10^{0}	0.0
300	1.02×10^{-4}	0.6
600	7.78×10^{-2}	6.2
900	8.16×10^{-1}	15.0

Analizing the results shown in tables 23, 24 and 25: The calculated Gibbs free energy ($\Delta_r G^\circ$) shows a decreasing trend with increasing temperature, indicating greater reaction spontaneity at higher temperatures. However, there are discrepancies with experimental values, particularly at 900 K, where the calculated value (1.52 kcal/mol) is higher than the experimental one (-4.8 kcal/mol), suggesting an overestimation of reaction stability.

The entropy change ($\Delta_r S^\circ$) is consistently higher in calculations than in experimental data, particularly at high temperatures. This suggests that the model might overestimate disorder contributions in the reaction.

The equilibrium constant (K_{eq}) follows the expected trend, increasing with temperature. However, the calculated values are lower than the experimental ones, indicating an underestimation of reaction spontaneity.

Overall, KiSThelP captures the qualitative behavior of thermodynamic properties but shows quantitative deviations.

We can also calculate the rate constant of the reaction using the transition state theory with KiSThelP. It can be calculated using the Eyring-Polanyi equation 10

$$k = \frac{\kappa k_B T}{h} e^{-\frac{\Delta G^\ddagger}{RT}} \tag{10}$$

Table 26: Rate constants for the reaction calculated using TST with KiSThelP and experimental data. All constants are in units of $\frac{cm^3}{molecule \cdot s}$.

T (K)	k (calculated)	k (exp.)
0.001	0.00	-
300	$7.60 \cdot 10^{-25}$	$5.80722 \cdot 10^{-18}$
600	$4.87 \cdot 10^{-18}$	$1.07385 \cdot 10^{-14}$
900	$1.41 \cdot 10^{-15}$	$2.0602 \cdot 10^{-13}$

As we can see in table 26 the calculated values are several orders of magnitude

The rate constant k follows an exponential dependence on the Gibbs free energy of activation $\Delta G^{\neq}$, even small deviations in its value lead to large variations in the computed rate constant. As previously observed in Table 23, the Gibbs free energy of activation calculated with KiSThelP deviates significantly from experimental values. This discrepancy directly impacts the predicted rate constants, resulting in values that differ by several orders of magnitude from experimental measurements.

4.5 Effect on the chemical equilibrium if the total pressure increases until 2 bar

Thermodynamic properties such as $\Delta G^\ddagger$, $\Delta_r G^\circ$, $\Delta_r S^\circ$, and K_{eq} are influenced solely by temperature and remain unaffected by pressure variations. However, alterations in pressure can impact the reaction's free energy, $\Delta_r G$, which depends on its standard value and the relative concentrations of reactants and products, as expressed in equation 11:

$$\Delta_r G = \Delta_r G^\circ + RT \ln Q \tag{11}$$

The reaction quotient, Q, represents the ratio of product and reactant concentrations and can be formulated for the studied reaction as follows:

$$Q = \frac{[CH_3][OH]}{[CH_4][O]} \tag{12}$$

Based on Le Châtelier's principle, an equilibrium system subjected to pressure variations will adjust to counteract that change. An increase in pressure, for instance, causes the reaction to shift in a direction that reduces the total number of gaseous molecules, thereby minimizing the pressure increase. In this particular case, increasing the pressure from 1 bar to 2 bar requires an assessment of the gaseous species on both sides of the reaction. Since the number of gas moles remains equal in both the reactants and the products, pressure changes

do not influence the equilibrium composition. Consequently, the system remains unaffected by pressure variations, as there is no net difference in gaseous molecules between the reactants and products.

4.6 Ocupation of O(^3P) Spin-Orbit Electronic States

The distribution of oxygen atoms among the three electronic levels that arise when spin–orbit coupling within its ground state term, ^3P. When coupling the orbital angular momentum $L = 1$ and spin $S = 1$ according to Russell–Saunders rules, three levels are obtained:

$$^3P_2, \quad ^3P_1, \quad \text{and} \quad ^3P_0,$$

where the subscript denotes the total angular momentum quantum number J, taking the values 2, 1, and 0, respectively.

The degeneracy of each level (i.e., the number of equivalent states) is given by

$$g_i = 2J + 1.$$

Thus, the degeneracies are:

$$g(^3P_2) = 5, \quad g(^3P_1) = 3, \quad g(^3P_0) = 1.$$

The experimental relative energies (in cm^{-1}) for these levels are:

$$^3P_2 : \ 0.000, \quad ^3P_1 : \ 158.265, \quad ^3P_0 : \ 226.977.$$

To determine the population of each electronic state at a fixed temperature T, the Boltzmann distribution is used. The probability p_i of an oxygen atom being in state i is given by:

$$p_i = \frac{g_i \, e^{-\varepsilon_i/(k_B T)}}{\sum_{n=1}^{3} g_n \, e^{-\varepsilon_n/(k_B T)}},$$

where ε_i is the energy of the ith state, and k_B is the Boltzmann constant. The partition function for the oxygen atom in the ^3P term is:

$$q = \sum_{i=1}^{3} g_i \, e^{-\varepsilon_i/(k_B T)}.$$

At $T = 0\,\mathrm{K}$, the thermal energy is insufficient to excite the atoms, so the exponential factors for the excited states vanish. Therefore, all atoms populate the ground state $^3P_2$:

$$p(^3P_2) = 1, \quad p(^3P_1) = 0, \quad p(^3P_0) = 0.$$

At a temperature of $T = 300\,\mathrm{K}$, the thermal energy allows a fraction of atoms to be excited to the $^3P_1$ and $^3P_0$ states, although the majority remain in $^3P_2$. According to the calculations, the populations are approximately:

$$p(^3P_2) \approx 0.74, \quad p(^3P_1) \approx 0.21, \quad p(^3P_0) \approx 0.05.$$

This analysis demonstrates how both the energy differences and the degeneracies influence the state populations at different temperatures, which is essential for accurately calculating thermodynamic properties.

4.7 Calculation of the molecules using symmetry in GAMESS

The CH_4 and CH_3 molecules exhibit well-defined symmetry, which influences their thermodynamic properties. CH_4 is fully symmetric, with equal bond lengths and tetrahedral angles of 109.47^{o}, belonging to the T_d symmetry group, meaning it adopts a perfect tetrahedral structure. Similarly, CH_3 has a D_{3h} symmetry group, with bond angles of 120^{o}, corresponding to a trigonal planar geometry. In previous calculations, the C_1 symmetry group was used, implying no symmetry consideration, which limits the accuracy of the obtained thermodynamic properties. By using GAMESS and incorporating the correct symmetry groups, it is possible to compute more precise thermodynamic properties.

Table 27: Partition functions (dimensionless) for CH_4 and CH_3 with and without symmetry.

T (K)	q no sym (CH_4)	q sym (CH_4)	q no sym (CH_3)	q sym (CH_3)
0.001	$1.39 \cdot 10^{-13}$	$1.16 \cdot 10^{-14}$	$1.46 \cdot 10^{-13}$	$2.43 \cdot 10^{-14}$
300	$1.13 \cdot 10^{9}$	$9.44 \cdot 10^{7}$	$1.37 \cdot 10^{9}$	$2.28 \cdot 10^{8}$
600	$2.12 \cdot 10^{10}$	$1.77 \cdot 10^{9}$	$3.17 \cdot 10^{10}$	$5.29 \cdot 10^{9}$
900	$1.58 \cdot 10^{11}$	$1.31 \cdot 10^{10}$	$2.44 \cdot 10^{11}$	$4.07 \cdot 10^{10}$

Regarding the partition function, the only contribution affected by symmetry is the rotational one. The results clearly show how the consideration of molecular symmetry modifies the partition function, particularly its rotational contribution. Consequently, the rotational partition function is divided by the symmetry number $\sigma = 12$. Likewise, for CH_3, which exhibits 120^{o} angles and a D_{3h} symmetry group, we have $\sigma = 6$. In previous calculations, a C_1 symmetry (i.e., no symmetry) was assumed, effectively setting $\sigma = 1$. This omission of symmetry leads to an overestimation of the partition function. By comparing the non-symmetric and symmetric results (for instance, dividing the "no sym" partition function by the "sym" one), we obtain the expected symmetry number. Hence, the only significantly affected contribution is the rotational one, as reflected in the tabulated values at different temperatures. Performing calculations in GAMESS that include the actual symmetry groups (T_d for CH_4 and D_{3h} for CH_3) yields more accurate thermodynamic properties because it corrects the overcounting that occurs when C_1 is assumed.

Table 28: Calculated frequencies for the symmetric CH_4 molecule.

Frequency (cm^{-1})	Symmetry	IR Intensity
14.973	T1	0
14.970	T1	0
14.960	T1	0
0.036	T2	0
0.010	T2	0
0.036	T2	0
1364.952	T2	0.32984
1364.952	T2	0.32984
1364.952	T2	0.32984
1582.617	E	0
1582.617	E	0
3073.886	A1	0
3210.779	T2	0.52103
3210.779	T2	0.52103
3210.779	T2	0.52103

Table 29: Calculated frequencies for the symmetric CH_3 radical.

Frequency (cm^{-1})	Symmetry	IR Intensity
5.983	E'	0
0.273	A2"	0
0.061	E'	0
9.875	E'	0
18.289	E"	0
18.289	E"	0
420.709	A2"	1.95268
1452.299	E'	0.06970
1452.299	E'	0.06970
3171.741	A1'	0
3363.785	E'	0.10528
3363.785	E'	0.10528

In this case the symmetry changes for the different vibrations unlike before where all of them had symmetry A.

Table 30: Variations of the Gibbs free energy of the reaction calculated taking into account the symmetry of CH_4 and CH_3.

T (K)	$\Delta_r G^\circ_{calc}$ (kcal/mol)	$\Delta_r G^\circ_{exp}$ (kcal/mol)
0.001	6.836	1.8
300	5.071	0.3
600	2.222	-2.2
900	-0.870	-4.8

The Gibbs free energy depends on the partition function as we can see in equation 13

$$G = -Nk_BT\left(\frac{\partial \ln q}{\partial N}\right)_{V,T} \tag{13}$$

When comparing the variation of the Gibbs free energy obtained for molecules without symmetry, we observe that incorporating symmetry significantly improves the alignment between calculated and experimental values. This suggests that the computation of the canonical partition function is more precise when symmetry considerations are included, leading to more accurate thermodynamic predictions such as ΔG°, ΔS° and K_{eq}.

5 Conclusions

Importance of Symmetry in Calculations: Proper consideration of molecular symmetry is crucial for improving the accuracy of computational results. If symmetry is not included (e.g., using a C1 point group, which ignores symmetry), certain contributions—especially rotational—are overestimated in the partition function. By incorporating the correct symmetry group for each molecule in the calculations, this overcounting of equivalent states is avoided, leading to thermodynamic properties (free energies, entropies, equilibrium constants, etc.) that align more closely with experimental values. In summary, respecting molecular symmetry in simulations enhances the fidelity and reliability of thermodynamic predictions.

Choice of Basis Sets and Computational Methods: The quality of the basis set and the computational method employed directly affects result accuracy. This study showed that a 6-311G(d,p) basis set combined with UMP2 provides reasonable results but tends to overestimate reaction energies compared to experimental data. Previous studies and higher-level calculations indicate that using larger basis sets (e.g., aug-cc-PVTZ, a triple-zeta set with diffuse functions) along with higher-order post-Hartree-Fock methods yields results much closer to experimental values. Thus, selecting high-quality basis sets and advanced electronic correlation methods is crucial for obtaining reliable thermodynamic predictions. This is evident in the fact that improving the basis set significantly reduces discrepancies in reaction and activation energies compared to expected values.

Impact of Approximations in the Partition Function: Assumptions made in calculating the partition function have a significant influence on derived thermodynamic properties. Standard thermodynamic calculations apply simplifications such as the ideal gas model, the rigid rotor for rotation, and the harmonic oscillator for vibration. While these models facilitate calculations, neglecting physical effects (such as anharmonicities, vibrational couplings, or molecular symmetries) can introduce errors. For example, an initial calculation ignored molecular symmetry ($\sigma = 1$), leading to an overestimation of the rotational contribution in the partition function for highly symmetric molecules like CH_4 and CH_3. Correcting this by dividing the rotational partition function by the appropriate symmetry number resulted in a lower partition function per molecule, yielding thermodynamic properties (such as Gibbs free energy) that better reflect reality. More generally, any approximation that does not fully capture all energy contributions of the system can cause deviations from experimental values. Therefore, careful evaluation of the assumptions used in the partition function is necessary, as it directly influences entropy, enthalpy, and free energy.

Sensitivity to Changes in Methods and Parameters: Finally, the high sensitivity of computational results to small changes in methods and parameters is highlighted. Even minor variations in the computational approach can lead to significant differences in the results. For instance, merely including or excluding symmetry in calculations alters the rotational partition function by factors corresponding to the symmetry number (for CH_4, a factor of 12), which in turn significantly affects calculated thermodynamic properties. Similarly, slight modifications in the choice of electronic method, basis set quality, or even numerical parameters such as convergence criteria can appreciably change the obtained energies and properties. This is evident in the fact that the calculated equilibrium constant (K_{eq}) showed large deviations from the experimental value due to its exponential dependence on the standard free energy change (ΔG°), which proved to be highly sensitive to corrections and the selected method. In conclusion, achieving reliable results requires strict control over these details: even a seemingly minor adjustment in calculation settings can have a substantial impact, making consistency and rigor in method and parameter selection essential for accurate thermodynamic calculations.

References

[1] Abas, N., & Kalair, A. R. (2015).*Futures, 69*, 31-49.

[2] Huarte-Larranaga, F., & Manthe, U. (2002). *The Journal of Chemical Physics, 117*(10), 4635-4638.

[3] Cremer, D. (2011). *WIREs Computational Molecular Science, 1*(4), 509-530.

[4] Schmidt, M. W., Baldridge, K. K., Boatz, J. A., Elbert, S. T., Gordon, M. S., Jensen, J. H., Koseki, S., Matsunaga, N., Nguyen, K. A., Su, S., Windus, T. L., Dupuis, M., & Montgomery, J. A. (1993). *Journal of Computational Chemistry, 14*(11), 1347-1363.

[5] Canneaux, S., Bohr, F., & Hénon, É. (2013). *Journal Of Computational Chemistry, 35*(1), 82-93.

[6] Chase, M. W. Jr., Ed. (1998). *J. Phys. Chem. Ref. Data, Monogr. 9*.

[7] González, M., Hernando, J., Millán, J., & Sayós, R. (1999). *The Journal Of Chemical Physics, 110*(15), 7326-7338.

[8] Miyoshi, A., Tsuchiya, K., Tezaki, A., & Matsui, H. (1995). *Springer eBooks* (pp. 131-136).